BIOCHEMISTRY
including biophysical chemistry & molecular biology

Article

pubs.acs.org/biochemistry

Improved Assays for Determining the Cytosolic Access of Peptides, Proteins, and Their Mimetics

Justin M. Holub,[†,∥] Jonathan R. LaRochelle,[‡,∥] Jacob S. Appelbaum,[§] and Alanna Schepartz*[,†,‡]

[†]Department of Chemistry, Yale University, P.O. Box 208107, New Haven, Connecticut 06520-8107, United States

[‡]Department of Molecular, Cellular and Developmental Biology, Yale University, P.O. Box 208103, New Haven, Connecticut 06520-8103, United States

[§]Department of Cell Biology, Yale University School of Medicine, P.O. Box 208002, New Haven, Connecticut 06520-8002, United States

Supporting Information

ABSTRACT: Proteins and other macromolecules that cross biological membranes have great potential as tools for research and next-generation therapeutics. Here, we describe two assays that effectively quantify the cytosolic localization of a number of previously reported peptides and protein domains. One assay, which we call GIGI (glucocorticoid-induced eGFP induction), is an amplified assay that informs on relative cytosolic access without the need for sophisticated imaging equipment or adherent cells. The second, GIGT (glucocorticoid-induced eGFP translocation), is a nonamplified assay that informs on relative cytosolic access and exploits sophisticated imaging equipment to facilitate high-content screens in live cells. Each assay was employed to quantify the cytosolic delivery of several canonical "cell permeable peptides," as well as more recently reported minimally cationic miniature proteins and zinc finger nuclease domains. Our results show definitively that both overall charge as well as charge distribution influence cytosolic access and that small protein domains containing a discrete, helical, penta-Arg motif can dramatically improve the cytosolic delivery of small folded proteins such as zinc finger domains. We anticipate that the assays described herein will prove useful to explore and discover the fundamental physicochemical and genetic properties that influence both the uptake and endosomal release of peptidic molecules and their mimetics.

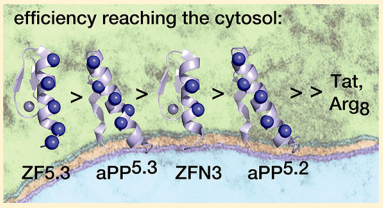

INTRODUCTION

There is great interest in the design and discovery of synthetic molecules that influence the functions of proteins within the cytosol and nucleus of living cells.[1−3] This interest is especially keen for proteins that are not enzymes, whose function depends not on covalent chemistry but rather on noncovalent interactions with other biomolecules: nucleic acids, lipids, or other proteins. Proteins that function in this manner constitute a significant fraction of the proteome but are notoriously difficult (albeit not impossible) to target with traditional, small molecule ligands.[4−7] By contrast, proteins that function through noncovalent interactions are effectively inhibited by peptides and small folded proteins, at least *in vitro*.[8,9] Unfortunately, despite the embodiment of highly favorable and evolvable attributes of Gibbs free energy, the size and polarity of most peptides and small proteins effectively prohibit passive diffusion across the plasma membrane.[10] As a result, peptides and small proteins rarely gain admittance to the cytosol, where innumerable protein·biomolecule interactions occur, and their tremendous promise as ligands for the "undruggable" proteome[2,11,12] remains frustratingly unfulfilled.

It has been known for over 40 years that addition of cationic charge to a peptide or protein can aid their uptake into cells.[13,14] More recently, it was discovered that peptides modified with α-methylated hydrocarbon staples,[15−17] as well as natural and engineered supercharged proteins[18−20] and some zinc finger nucleases[21−25] can, in certain cases and with varying levels of efficiency, find their way into the cytosol and nucleus. Although unquestionably condition dependent,[26] cell uptake in these cases generally proceeds not via passive diffusion, at least at low concentration.[27] Instead, uptake proceeds via the ubiquitous and interdependent processes of receptor-mediated endocytosis and endosomal release.[28−30] Unfortunately, most cationic peptides and proteins that engage the endocytic machinery remain trapped within vesicles where they are topologically separated from the cell interior and unable to access targets in the cytosol or nucleus.[31] Intracellular function, when observed, is believed to result from the mechanistically indistinct, unpredictable, and inefficient process of endosomal escape.

In accord with these early findings, we reported previously that small, pancreatic fold proteins containing between four and six cationic charges, arginine side chains, embedded within an α- or PPII-helix (Figure 1) are taken up efficiently by cells into endocytic vesicles.[32,33] Endocytic uptake is favored when the arginines are clustered on an α-helix within the context of a folded protein structure and is achieved without significant cytotoxicity. We reported more recently that although many

Received: August 6, 2013
Revised: October 14, 2013

   dx.doi.org/10.1021/bi401069g | *Biochemistry* XXXX, XXX, XXX−XXX

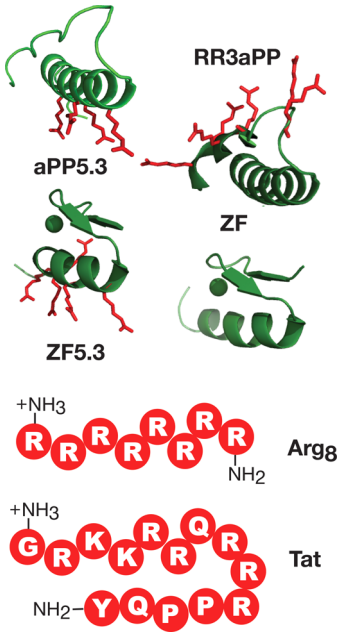

Figure 1. Examples of the peptides and protein domains evaluated in this work. Arginine side chains are shown explicitly in those molecules drawn as ribbons.[32,33]

pancreatic fold proteins containing four to six embedded arginines reach endocytic vesicles, very few reach the cytosol.[34] Endosomal release is favored by a distinct molecular signal encoded by five dispersed but precisely arrayed arginines on an α-helix, a penta-Arg motif.[34] The penta-Arg motif is transportable into diverse protein contexts and specifies release from vesicles characterized by the guanosine triphosphatase (GTPase) Rab5.[34]

In this work, we describe two assays that were developed to help explore the structural and genetic factors that control the release of penta-Arg-containing peptides, proteins, and peptide mimetics into the cytosol. In the past, identifying these factors has been constrained by the absence of rapid, robust, cell-based assays that effectively differentiate between molecules trapped within endocytic vesicles and those that escape into the cytosol.[31,36,37] The two assays described herein are complementary. One, which we refer to as GIGI, for glucocorticoid-induced eGFP induction (Figure 2a), is an amplified assay that informs on relative cytosolic access without the need for sophisticated imaging equipment or adherent cells. Because the GIGI signal is amplified by transcription and translation, this assay is especially useful when evaluating molecules whose ability to access the cytosol is low.

The second assay, which we refer to as GIGT, for glucocorticoid-induced eGFP translocation (Figure 2b), is a nonamplified assay that informs on relative cytosolic access in a manner that exploits sophisticated imaging equipment. It is uniquely suited to evaluate how the trafficking of a single molecule changes in the context of genomic si/shRNA knockdown screens in living cells. We then apply these assays to compare the localization of a number of previously reported molecules of diverse structure, including the canonical "cell-penetrating peptides" Tat and Arg_8, as well as miniature proteins and zinc finger domains.

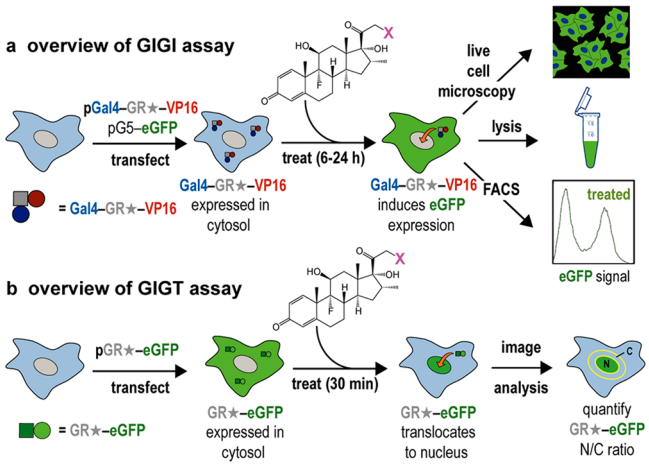

Figure 2. Overview of GIGI and GIGT assays for monitoring cytosolic localization of Dex-tagged peptides and proteins. (a) GIGI: glucocorticoid-induced eGFP induction. Cells are transfected (transiently or stably) with plasmids pG5-eGFP and pGal4-GR★-VP16 and treated with the glucocorticoid receptor (GR) ligand dexamethasone (Dex) or a conjugate thereof to induce the transcription and subsequent translation of eGFP. Relative eGFP levels are assessed by fluorimetry of lysed cells or by microscopy or FACS analysis of living cells. (b) GIGT: glucocorticoid-induced eGFP translocation. Cells are transfected (transiently or stably) with pk7-GR★-GFP and treated with Dex or a conjugate thereof to induce the nuclear translocation of GR★-GFP. The nuclear to cytoplasmic ratio of living cells is determined using fluorescence microscopy and high content image analysis software such as CellProfiler[35] or Acapella.

EXPERIMENTAL PROCEDURES

Quantifying GIGI in Cell Lysates. Cells were transfected with GIGI component plasmids (see Supporting Information) and transferred immediately to either full DMEM (for HeLa or HEK293T cells) or full McCoy's 5A (for U2OS cells) media that in certain cases was supplemented with the indicated Dex-conjugate. Cells were incubated with ligand for 24 h at 37 °C under 5% CO_2 before analysis. To reduce background, stable U2OS(GIGI) cells were switched to McCoy's 5A media supplemented with 5% charcoal-stripped FBS and penicillin/streptomycin (CS-5A) 24 h before the addition of ligand. Following incubation, the treatment medium was removed, and the cells were lysed in 1× RIPA buffer (0.5 M Tris-HCl, pH 7.4, 1.5 M NaCl, 2.5% deoxycholic acid, 10% NP-40, and 10 mM EDTA) (Millipore, #20-188) containing 1× EDTA-free protease inhibitor (Roche, #11836170001) at room temperature for 15 min in the dark. Fluorescence intensities of each volume of the cell lysate were quantified using a fluorescence plate reader (Analyst AD, LJL Biosystems). To measure eGFP fluorescence intensity, excitation and emission wavelengths were set to 485 and 530 nm, respectively. To measure RFP fluorescence intensity, excitation and emission wavelengths were set to 530 and 580 nm, respectively. Relative fluorescence units (RFUs) were calculated as shown in eq 1, and dose–response curves are represented by the best fit of the data to eq 2. RFUs are expressed ± standard deviation (Excel). The maximum induction level is defined as RFU_{max}. Data were processed using Kaleidagraph and GraphPad Prism software.

$$RFU = ([I_{530}]/[I_{580}]) - ([I'_{530}]/[I'_{580}]) \quad (1)$$

$[I_{530}]$ = fluorescence intensity at 530 nm in treated cells, $[I_{580}]$ = fluorescence intensity at 580 nm in treated cells, $[I'_{530}]$ =

dx.doi.org/10.1021/bi401069g | Biochemistry XXXX, XXX, XXX–XXX

fluorescence intensity at 530 nm in untreated cells, and $[I'_{580}]$ = fluorescence intensity at 580 nm in untreated cells.

$$Y = Y_{min} + (Y_{max} - Y_{min})/(1 + 10^{logEC50-X}) \quad (2)$$

Y is relative fluorescence units (RFU) or translocation ratio (TR), Y_{max} and Y_{min} are the maximal and minimal values at each concentration of ligand, X is the [ligand], and EC_{50} is the ligand concentration that corresponds to $Y_{max}/2$.

Epifluorescence Microscopy (GIGI). Cells were plated at a density of 10,000 cells/well in full DMEM (HeLa or HEK293T) or full McCoy's 5A (U2OS or U2OS(GIGI)) on 96-well glass bottom plates (Matrical Bioscience, #MGB096-1-2-LG-L) and allowed to adhere overnight. For transient GIGI assays, the cells were transfected as described (see Supporting Information). Following transfection, the cells were immediately switched to full DMEM (HeLa and HEK293T) or full McCoy's 5A (U2OS) supplemented with or without ligand as indicated and were allowed to incubate for 24 h at 37 °C under 5% CO_2. To reduce background, stable U2OS(GIGI) cells were switched to CS-5A media 24 h before the addition of the ligand. Following treatment, the cells were washed with PBS (Life Technologies, #14190-144), and the nuclei were stained by treating the cells with 1 μg/mL Hoechst 33342 (Molecular Probes, #H3570) in full media for 10 min at 37 °C under 5% CO_2. The cells were then washed with PBS and overlaid with HEPES−Krebs−Ringer's (HKR) buffer (140 mM NaCl, 2 mM KCl, 1 mM $CaCl_2$, 1 mM $MgCl_2$, and 10 mM HEPES at pH 7.4) and imaged using a Zeiss Axiovert 200 M epifluorescence microscope outfitted with a Ziess Axiocam MRm camera. Fluorescence illumination was initiated using an EXFO X-cite Series 120 Hg arc lamp. Hoechst 33342 images were acquired using the Zeiss Filter Set #49 (excitation G 365 nm, FT 395, emission BP 445/50), and GFP images were acquired using Zeiss Filter Set #44 (excitation BP 475/50 nm, FT 500, emission BP 530/50 nm). Images were processed using AxioVision 4.8 and ImageJ[39] software.

FACS Analysis (GIGI). Cells were plated at 50,000 cells/well in full DMEM (HeLa or HEK293T) or full McCoy's 5A (U2OS or U2OS(GIGI)) on 12-well plates (Corning, #3043) and allowed to adhere overnight at 37 °C under 5% CO_2. For transient GIGI assays, cells were transfected as described (see Supporting Information). Following transfection, the cells were immediately switched to full DMEM (HeLa and HEK293T) or full McCoy's 5A (U2OS) supplemented with or without ligand as indicated and were allowed to incubate for 24 h at 37 °C under 5% CO_2. To reduce background, stable U2OS(GIGI) cells were switched to CS-5A media 24 h before the addition of the ligand. Once treatments were complete, the cells were washed with PBS and lifted off the plate with 0.25% trypsin in 1 mM EDTA (Life Technologies, #25200-056). The cells were then resuspended in full DMEM (HEK293T or HeLa), full McCoy's 5A (U2OS) or CS-5A (U2OS(GIGI)), transferred to fresh microfuge tubes (USA Scientific, #1415-2600), and pelleted by centrifugation. After the media were aspirated, the cells were washed with ice cold PBS and pelleted again by centrifugation. The wash solution was aspirated, and the cells were resuspended in ice cold PBS. Cells were then counted using flow cytometetry (Accuri C6, BD, San Jose, CA) recording 20,000 events for each experiment. Excitation and emission wavelengths were set to 488 and 533 nm, respectively. Data were gated to include cell populations of viable cells using forward scatter and side scatter filters. Gating was also performed to exclude background fluorescence as determined from untreated cells. Relative emission levels were quantified from histograms plotting count vs fluorescence intensity. Data were processed using FlowJo, Kaleidagraph, and GraphPad Prism software.

Quantifying GIGT in Live Cells. Following transfection (see Supporting Information), cells were transferred immediately to clear DMEM (Life Technologies, #21063-029) supplemented with or without Dex ligand and 300 nM Hoechst 33342. Cells were allowed to incubate in the presence of ligand for 30 min at 37 °C under 5% CO_2. Once the incubation was complete, the media were replaced with HKR imaging buffer, and the cells were imaged using a Zeiss Axiovert 200 M epifluorescence microscope outfitted with a Ziess Axiocam MRm camera. Fluorescence illumination was initiated using an EXFO X-cite Series 120 Hg arc lamp. Hoechst 33342 images were acquired using the Zeiss Filter Set #49 (excitation G 365 nm, FT 395, emission BP 445/50), and GFP images were acquired using Zeiss Filter Set #44 (excitation BP 475/50 nm, FT 500, emission BP 530/50 nm). Fluorescence intensities of individual cells were quantified using the image analysis algorithm CellProfiler (see Supporting Information).

High-Content Imaging of GIGT in Saos2(GIGT) Cells. Saos2(GIGT) cells were plated onto 384-well plates (2,500 cells/well) in 40 μL of full McCoy's 5A and allowed to adhere overnight. To reduce background translocation, the plating media were removed, and cells were overlaid with clear DMEM (Life Technologies, #21063-029) for 16 h before treatment. Clear DMEM supplemented with ligand (5× concentration, 10 μL) was then added directly to the wells, and the cells were allowed to incubate for 30 min. Following treatment, cells were fixed with 4% paraformaldehyde for 20 min at room temperature and washed with PBS. For imaging, the cells were counter-stained with Hoechst 33342 for 30 min at room temperature and imaged on an Opera high content screening system (PerkinElmer Life and Analytical Sciences) using a 20 × 0.45 NA lens. GR★-eGFP fluorescence was detected using a solid state 488 nm laser and a 540/75 bandpass filter, while Hoechst 33342 was detected using a 405 nm laser and a 450/50 bandpass filter. Translocation ratios were determined using Acapella high content imaging and analysis software, with a script that processed the images in a manner similar to the CellProfiler pipeline described in the Supporting Information. Each data point represents 30−60 images containing over 100 cells.

***Z′*-Factor Determination.** The Z'-factor[38] is a statistical parameter that is used to quantify the suitability of an assay for use in high-throughput screening. The Z'-factor measures the statistical separation of the means and standard deviations between treated and untreated cell populations. A negative Z'-factor value results from substantial overlap between positive and negative control samples and is indicative of a weak assay. More robust separation between the sample populations gives positive Z'-factor values, approaching 1 as separation increases toward infinity. Values were calculated using eq 3 and were determined for GIGI and GIGT experiments with sample sizes ranging from n = 60 to 150.

$$Z' - factor = 1 - (3(\sigma_1 + \sigma_2/|\mu_1 - \mu_2|) \quad (3)$$

In eq 3, σ_1 is the standard deviation of the treated sample, σ_2 is the standard deviation of the untreated sample (control), μ_1 is the mean of the treated sample, and μ_2 is the mean of the untreated sample (control).[38]

dx.doi.org/10.1021/bi401069g | Biochemistry XXXX, XXX, XXX−XXX

RESULTS

Developing Methodology: GIGI Design and Rationale. The design of GIGI (Figure 2a) began with an assay reported almost a decade ago by Kodadek and co-workers.[40] In this assay, cells are transfected with a plasmid encoding an artificial transcription factor composed of a glucocorticoid receptor ligand-binding domain (GR), a Gal4 DNA binding domain (Gal4), and a VP16 transactivation domain (VP16). Cells are also transfected with plasmids encoding a Gal4-driven firefly luciferase reporter gene and a constitutively active *Renilla reniformis* luciferase gene as an internal control.[40] In the absence of a glucocorticoid ligand (such as Dex or a Dex-tagged peptide or peptide mimetic), the Gal4-GR-VP16 fusion protein remains trapped in the cytosol by tight interactions between the GR and Hsp90 and other chaperones.[41,42] Appearance of glucocorticoid in the cytosol releases these chaperones and reveals nuclear localization sequences within the GR LBD.[43,44] The subsequent nuclear translocation of the Gal4-GR-VP16 fusion protein activates the expression of a Gal4-driven luciferase reporter gene.[40,45] Because the Gal4-GR-VP16 fusion protein traffics to the nucleus and directs luciferase expression only after direct binding to a Dex-tagged molecule in the cytosol, this technique can be, and has been, used to detect the cytosolic delivery of Dex-tagged peptides and peptide mimetics.[40,45−47] We note, however, that this assay alone does not provide information about the pathway by which a molecule finds its way into the cytosol; additional experimentation is required to differentiate between molecules that diffuse directly across the plasma membrane and those that hijack the endocytic machinery.

Although useful and convenient for evaluating compound libraries of modest size, the assay described by Yu et al. does not adapt easily to genomic libraries or live cell visualization. First, the readout is slow. Up to 40 h is required to accumulate measurable levels of luciferase, which hinders its application to small molecule or RNA interference (RNAi) screens that operate on shorter time scales. Second, the assay is costly. The luciferase substrate is expensive, and the reagents needed to perform the assay in 384-well format cost in excess of $100 per plate. This high cost further discourages application of this assay to screen tens of thousands of samples in high-throughput. Finally, it is now well-known that assays based on luciferase activity can be confounded by false positive signals that result from the stabilization of luciferase by allosteric inhibitors.[48]

Here, we describe a number of simple but effective modifications to the assay described by Yu et al. that overcome all three of these limitations in the context of two complementary assays. The first modification replaces the wild-type GR in the Gal4-GR-VP16 fusion protein with a variant, termed GR★, which possesses significantly improved affinity for Dex and Dex-tagged materials.[49,50] The second modification replaces the Gal4-driven luciferase reporter gene with one encoding eGFP. These changes reduce the measurement time from 40 h to 6−24 h, eliminate the need for costly luciferase substrates, abolish concerns about false activation by allosteric inhibitors,[48] and allows the assay to be performed in living cells. The third change, embodied in the assay we refer to as GIGT (vide infra), increases speed even more, to 30 min, by dispensing entirely with transcription and translation and instead directly quantifies the translocation of a GR★ fusion from the cytosol to the nucleus of living cells (Figure 2b).

Development of GIGI. First, we sought to verify that cell lines expressing the reported Gal4−GR−VP16 fusion protein[40,45] would express eGFP upon treatment with a GR ligand. We transiently transfected three widely used cell lines, U2OS, HeLa, and HEK293T, with pGal4−GR−VP16,[40,45] as well as with plasmids encoding the Gal4-driven eGFP reporter plasmid (pG5-eGFP) (see Supporting Information) and a constitutively active mCherry (pmCherry-N1) to provide a measurable control for transfection efficiency and cell viability. Following transfection, cells were treated for 24 h with 1 or 10 μM of the glucocorticoid dexamethasone-21-thiopropionic acid (SDex).[45,46] The cells were then lysed, and relative eGFP expression levels, conveyed as relative fluorescence units (RFUs), were determined (Figure 3a). Treatment of HeLa and HEK293T cells expressing the GIGI system with 1 or 10 μM SDex[45] led to moderate to strong eGFP expression, whereas lower expression was observed in U2OS cells. Despite these variations, all cells expressed significant levels of eGFP upon treatment with SDex, suggesting that the GIGI assay could be performed in multiple commonly utilized cell lines. To

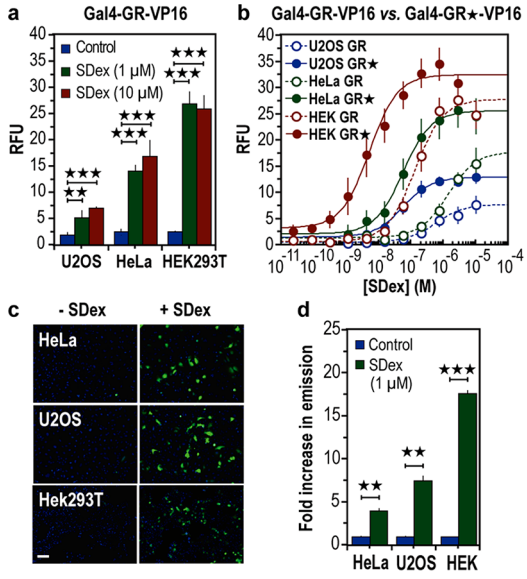

Figure 3. GIGI validation. (a) GIGI in lysates: comparison of eGFP expression in U2OS, HeLa, and HEK293T cells transiently transfected with pGal4-GR-VP16, pG5-eGFP and pmCherry-N1 and treated with SDex or without (control). (b) GIGI in lysates: comparison of eGFP expression in lysates of cells transiently transfected with pG5-eGFP, pmCherry-N1, and either pGal4-GR-VP16 or pGal4-GR★-VP16, treated with varying concentrations of SDex. RFU values were calculated from individual wells using eq 1 (see Experimental Procedures) and are expressed ± standard deviation (Excel). Curves shown represent the best fit of the data to eq 2 (see Experimental Procedures). (c) GIGI in living cells: live-cell imaging of eGFP expression in three transiently transfected cell lines. Cells were incubated in the presence or absence of 1 μM SDex for 24 h before imaging by epifluorescence microscopy. Nuclei were stained using Hoechst 33342. Scale bar = 50 μm. (d) GIGI in living cells: quantification of eGFP expression by FACS analysis in transiently transfected HeLa, U2OS, and HEK293T cells treated for 24 h with 1 μM SDex. The mean cellular fluorescence for untreated (control) transfectants was set to 1, and other values are expressed as the fold-increase in fluorescence emission at 533 nm ± standard deviation (Excel). For panels a and d, statistical analysis was performed using a two-tailed Student's t test with each cell line treated as a separate population; ** $p \leq 0.005$, *** $p \leq 0.001$.

dx.doi.org/10.1021/bi401069g | *Biochemistry* XXXX, XXX, XXX−XXX

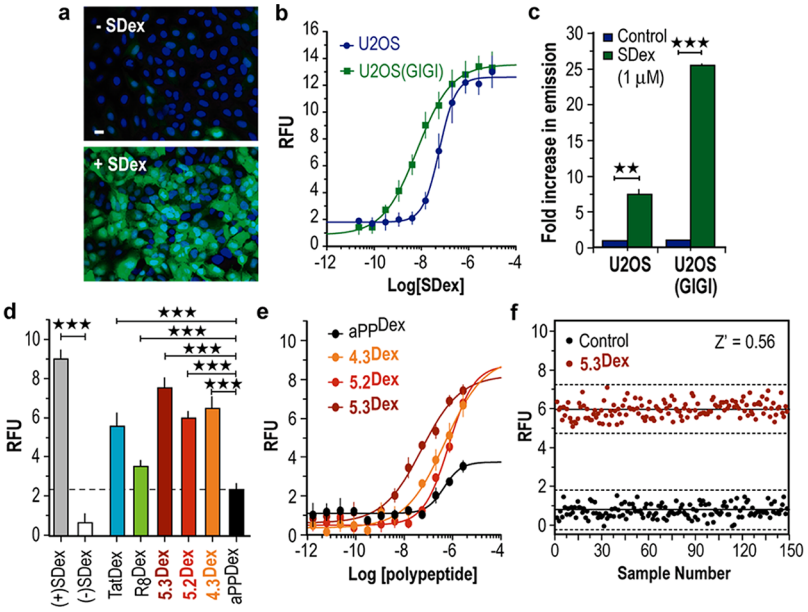

Figure 4. GIGI assays performed in stably transfected U2OS(GIGI) cells. In all cases, RFUs were calculated using eq 1 (see Experimental Procedures) and are expressed ± standard deviation (Excel). Curves shown represent the best fit of the data to eq 2 (see Experimental Procedures). Statistical analysis was performed using a two-tailed Student's *t* test with each cell line treated as a separate population; ** $p \leq 0.005$, *** $p \leq 0.001$. (a) GIGI in live cells: live-cell epifluorescent imaging of U2OS(GIGI) cells treated for 24 h with or without 1 μM SDex. Nuclei were stained with Hoechst 33342. Scale bar = 20 μm. (b) GIGI in lysates: comparison of eGFP expression in lysates prepared from transiently transfected U2OS and U2OS(GIGI) cells treated with varying concentrations of SDex for 24 h. (c) GIGI in live cells: quantification of eGFP expression by FACS analysis in transiently transfected U2OS and U2OS(GIGI) cells treated for 24 h with or without 1 μM SDex. The mean cellular fluorescence for untreated (control) transfectants was set to 1, and other values are expressed as the fold-increase in fluorescence emission at 533 nm ± standard deviation. (d) GIGI in lysates: relative eGFP expression levels in U2OS(GIGI) cells treated with 1 μM of the indicated Dex-tagged miniature protein or peptide. (e) GIGI in lysates: concentration-dependent effect of each miniature protein on eGFP expression in U2OS(GIGI) cells. EC_{50} values are shown in Table S2f, Supporting Information) GIGI in lysates: well-to-well variability of GIGI in U2OS(GIGI) cells treated with 1 μM 5.3^{Dex} or without (control). Randomized RFU values were then plotted as a function of sample number; n = 150. Solid lines represent mean RFUs for treated or untreated cells. Dashed lines represent the mean value ± 3 times the standard deviation (Excel). The Z'-factor[38] was calculated using eq 3 (see Experimental Procedures).

determine whether we could detect eGFP in transiently transfected cells at treatment times less than 24 h, we treated HeLa or HEK293T cells with 1 μM SDex for various times between 30 min to 24 h. Following treatment, the cells were lysed, and relative eGFP expression levels were determined as described above (Figure S1, Supporting Information). Significant eGFP levels were measured in HEK293T cells after 6 h, whereas 24 h were required in HeLa cells.

Improving Sensitivity with a Super GR Variant. Many glucocorticoid receptor variants have been prepared to study the contributions of individual amino acids to steroid affinity, ligand selectivity, and transcriptional activity.[49−52] One widely studied variant contains a single cysteine to glycine substitution within the ligand-binding domain, at position 656 of the rat GR. The C656 side chain is located near the entrance to the steroid binding pocket and clashes with the steroid C-20 carbonyl oxygen.[49,50] Previous work has shown that, *in vitro*, rat C656G GR binds Dex with an equilibrium dissociation constant (K_d) of 0.55 nM, about 10-fold more tightly than the wild-type GR ligand-binding domain.[49] In cultured H4IIE cells, a similarly mutated full-length GR activated target gene transcription at a 500-fold lower Dex concentration than did the wild-type receptor.[51] On the basis of these results, we hypothesized that installing the C656G substitution within the Gal4-GR-VP16 fusion protein, to generate Gal4-GR★-VP16, would increase the sensitivity with which Dex-tagged molecules could be detected in the cytosol.

To test this hypothesis, HeLa, U2OS, and HEK293T cells were transiently transfected with plasmids encoding either Gal4-GR-VP16 or Gal4-GR★-VP16 (see Supporting Information), along with pG5-eGFP and pmCherry-N1, and treated with between 10^{-11} and 10^{-5} M SDex. After 24 h, the cells were lysed and relative eGFP expression levels, conveyed as relative fluorescence units (RFU), were quantified.

As shown in Figure 3b, in all cases eGFP production increased with ligand concentration, and the midpoint of the response curve (EC_{50}) was significantly lower when eGFP production was driven by Gal4-GR★-VP16. The effect of the GR★ mutation was most dramatic in HEK293T and HeLa cells, with as much as a 30-fold decrease in EC_{50}; lower fold-changes and overall expression levels were observed in U2OS cells (Table S1, Supporting Information). HeLa cells transfected with Gal4-GR-VP16 or Gal4-GR★-VP16 were characterized by EC_{50} values of 771 nM and 30 nM, respectively; the corresponding values for U2OS cells were 577 nM and 44 nM, and 256 nM and 3 nM for HEK293T cells. Western blot experiments in HEK293T and HeLa cells confirmed that the observed fluorescence signals resulted from SDex-induced eGFP expression (Figure S2, Supporting Information).

GIGI Quantified by Live Cell Imaging. Next, we asked whether we could use GIGI to evaluate the cytosolic access of Dex-tagged molecules without the need for cell lysis, that is, in living cells. HeLa, U2OS, and HEK293T cells were each transiently transfected with pGal4-GR★-VP16, pG5-eGFP, and pmCherry-N1, treated with or without 1 μM SDex, and

dx.doi.org/10.1021/bi401069g | *Biochemistry* XXXX, XXX, XXX−XXX

examined using epifluorescence microscopy or flow cytometry. All cell lines tested showed significant SDex-dependent increases in eGFP fluorescence, whether viewed by microscopy (Figure 3c) or analyzed by flow cytometry (Figures 3d and S3, Supporting Information). Using flow cytometry, the fold increase in eGFP expression was greatest in HEK293T cells (18-fold), followed by U2OS cells (8-fold), and then by HeLa cells (4-fold). This order is slightly different than that observed when eGFP expression was analyzed after cell lysis (see Figure 3b). In both cases, HEK293T cells show the greatest increase in eGFP production in the presence of SDex, while the relative increases in eGFP expression in HeLa and U2OS cells differ, perhaps because of the higher inherent autofluorescence of HeLa cells[53] or the larger cell size of U2OS cells.[54] Control experiments verified that the observed difference in fold-induction did not result from differences in transfection efficiency (Figure S4 and Table S1, Supporting Information).

Establishing a Stable GIGI Reporter System in U2OS Cells. The working time frame of assays that utilize transiently transfected cells is limited, as transfected plasmids and expressed proteins can be rapidly degraded.[55] Indeed, the GIGI assay was time-sensitive in transiently transfected HEK293T cells, with signal levels reduced to near background levels after 72 h (Figure S5, Supporting Information). We hypothesized that a cell line stably transfected with GIGI components would eliminate this time dependence and facilitate the application of this system to high-throughput screening, which is most robust in stably transfected cells.[55]

To test this hypothesis, we first used standard antibiotic resistance methods to select for U2OS cells that were stably transfected with GIGI components derived from pG5-eGFP, pGal4-GR★-VP16, and pmCherry-N1 (see Supporting Information, Figure S6) and dubbed this new cell line U2OS(GIGI). We observed no difference in the viability or morphology of U2OS and U2OS(GIGI) cells over several weeks of growth, suggesting that the cells can tolerate long-term expression of Gal4-GR★-VP16. To ensure that the GIGI assay would perform in U2OS(GIGI) cells, we treated the cells for 24 h with or without 1 μM SDex and compared the levels of eGFP produced using epifluorescence microscopy (Figure 4a). Addition of 1 μM SDex to U2OS(GIGI) cells led to significant eGFP expression in greater than 85% of cells examined, a value much greater than the 19% efficiency observed in transiently transfected U2OS cells (compare Figures 3c and 4a, and Figure S7 and Table S1, Supporting Information). Furthermore, examination of the relative fluorescence of the two cell populations treated with between 10^{-11} to 10^{-5} M SDex after lysis indicated a significant improvement in EC_{50} from 58 nM for the transiently transfected U2OS cells to 6 nM for U2OS(GIGI) cells (Figure 4b and Table S1, Supporting Information). Finally, FACS analysis of transiently transfected U2OS or U2OS(GIGI) cells treated with 1 μM SDex showed the stably transfected cells to be roughly 3-fold brighter than the transient transfectants (Figure 4c). Taken together, these data indicate that U2OS(GIGI) cells represent a significant improvement in sensitivity and temporal control of the GIGI assay over transiently transfected U2OS cells.

Applying Methodology: Using GIGI to Evaluate Cytosolic Delivery. Next, we made use of U2OS(GIGI) cells to compare the relative cytosolic delivery of Dex-tagged versions of the canonical cell-penetrating peptides Tat[56−58] and octaarginine (Arg_8)[59−61] as well as a series of previously examined minimally cationic pancreatic fold proteins (see Supporting Information and Table S2)[33,34] (Figure 4d). Examined after treatment and cell lysis, we observed significant eGFP expression in U2OS(GIGI) cells treated with 1 μM Tat^{Dex}, $Arg_8{}^{Dex}$, 5.3^{Dex}, 5.2^{Dex}, and 4.3^{Dex}, with the highest levels produced in the presence of 5.3^{Dex}. The superiority of 5.3^{Dex} was also observed using a previously reported translocation assay using GR-GFP[34] (the predecessor of GIGT). Notably, two peptides that did not induce eGFP expression in transiently transfected HeLa cells, 5.2^{Dex} and 4.3^{Dex} (Figure S8, Supporting Information), led to significant expression across a wide concentration range in U2OS(GIGI) cells (Figure 4e), highlighting the increased sensitivity in U2OS(GIGI) cells for evaluating the cytosolic delivery of Dex-labeled material. The EC_{50} for cells treated with 5.3^{Dex} is 52.9 nM, a value approximately 10-fold lower than that of the next most potent peptide, 4.3^{Dex} (EC_{50} = 482.1 nM). EC_{50} values for all peptides described herein are shown in Table S3, Supporting Information.

Finally, to test the well-to-well variability of an assay performed in U2OS(GIGI) cells, we treated a large sample population (n = 150) with or without 1 μM 5.3^{Dex} for 24 h and quantified eGFP expression from cell lysates (Figure 4f). The Z'-factor is a statistical parameter that is used to quantify the suitability of an assay for use in high-throughput screening and provides a measure of the amount of separation between two sample populations.(see eq 3 in Experimental Procedures)[38] A negative Z'-factor results from substantial overlap between positive and negative control samples, while the Z'-factor approaches 1 as separation increases toward infinity. The Z'-factor measured for the GIGI assay in the presence of 5.3^{Dex} was 0.56 across 150 wells, a value that indicates that GIGI is robust enough to be used for high-throughput screening of cell populations treated with 5.3^{Dex}.

Developing Methodology: GIGT Design and Rationale. While GIGI eliminates many disadvantages of the assay reported by Yu et al.,[40] it is still limited by the time delay between the entry of Dex-tagged molecules into the cytosol and eGFP expression. Previously, we made use of an assay that minimized this delay by monitoring the nuclear translocation of a GR-GFP fusion protein, as opposed to its expression, and applied this assay to evaluate the relative cytosolic levels of Dex-tagged peptides and proteins.[34] We hypothesized that the sensitivity of this nuclear translocation assay would also be improved by introduction of the C to G mutation within the GR ligand-binding domain, generating GR★-GFP (see Supporting Information).

To test this hypothesis, we expressed either GR-GFP or GR★-GFP in HeLa and U2OS cells, and monitored the nuclear translocation of each construct in the presence and absence of 100 nM SDex (Figure 5a) by epifluorescence microscopy. Nuclear translocation was quantified by measuring the ratio of the mean GFP signal in the nucleus to the mean signal within the surrounding cytosol using CellProfiler[35] (see Supporting Information). In both cell lines, replacing GR-GFP with GR★-GFP led to a significant decrease in the SDex concentration required to achieve the half maximal translocation ratio (TR). This concentration decreased from 171 nM to 22 nM in HeLa cells and from 639 nM to 162 nM in U2OS cells, representing 8- and 4-fold improvements in sensitivity, respectively (Figure 5b and Table S4, Supporting Information).

Finally, we exposed cells expressing GR★-GFP to a series of Dex-tagged miniature proteins[34] as well as Tat^{Dex56} and

dx.doi.org/10.1021/bi401069g | Biochemistry XXXX, XXX, XXX−XXX

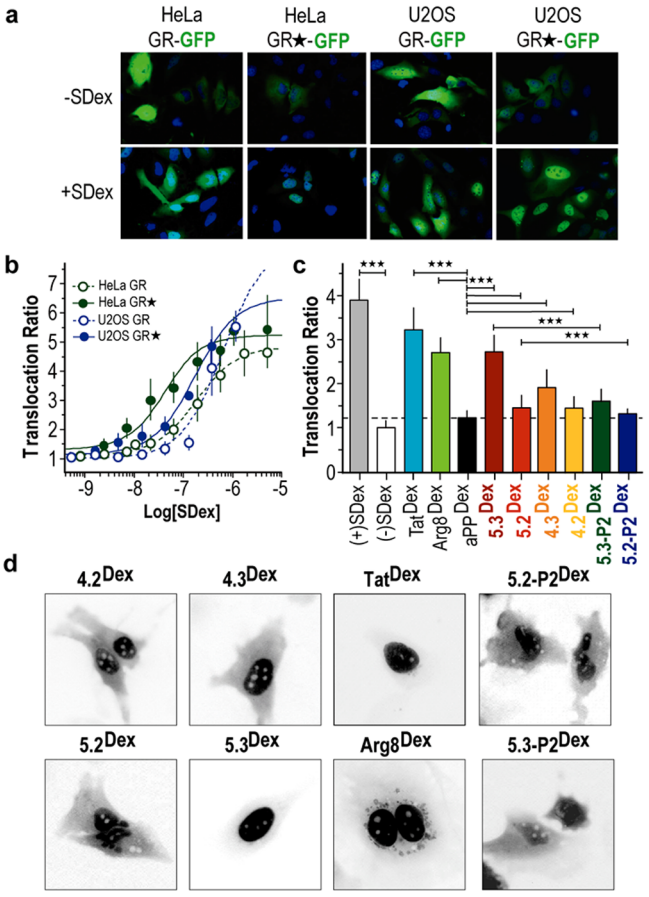

Figure 5. Validation of the GIGT assay in transiently transfected cells. (a) Images of HeLa and U2OS cells transiently transfected with GR-GFP or GR★-GFP with or without treatment with 100 nM SDex for 30 min. Images show an overlay of GFP signal (green) and Hoechst 33342 (blue). (b) Comparison of GR-GFP and GR★-GFP nuclear translocation values across varying SDex concentrations after 30 min of treatment. TRs, expressed ± standard deviation, were calculated using CellProfiler as previously reported[34] (see Supporting Information), and curves represent best fit of the data shown in eq 2 (see Experimental Procedures). (c) Analysis of GR★-GFP nuclear translocation in live HeLa cells with or without treatment with 500 nM SDex or Dex-labeled peptides for 30 min. *** $p \leq 0.001$, ANOVA. (d) Images of live HeLa cells treated with 500 nM Dex-tagged peptides for 30 min. GFP signal is shown in grayscale.

Arg_8^{Dex},[59] which have been evaluated previously on the basis of GR-GFP translocation[34] (Figure 4c and d). At 500 nM, which is one-half the ligand concentration previously tested,[34] the TRs measured in HeLa cells expressing GR★-GFP are similar to the those observed in HeLa cells expressing GR-GFP. In both cases among the miniature proteins, the highest TR values (2.79) were observed for cells treated with 5.3^{Dex}.[34] Structural variants of 5.3^{Dex} and 5.2^{Dex} containing proline substitutions at two positions within the α-helix (at positions F24 and Y31)[62] were also examined using GIGT. Treatment of cells expressing GR★-GFP with 5.3-$P2^{Dex}$ led to a significant decrease in TR when compared to that of its structured counterpart, from 2.79 ± 0.39 to 1.64 ± 0.27, as did treatment with 5.2-$P2^{Dex}$ (from 1.86 ± 0.36 to 1.35 ± 0.11) (Figures 4c and d). These changes provide additional evidence that efficient cytosolic entry of cationic miniature proteins requires a precise α-helical display of arginine residues.

Establishing a Stable GIGT Reporter System in Saos2 Cells. We hypothesized that a cell line stably transfected with GR★-GFP would allow the GIGT assay to be bridged with high-content imaging.[55] We chose human osteosarcoma Saos2 cells (ATCC, HTB-85) because their amenability to stable genetic modulation makes them ideal for constructing cell-based reporter systems.[63] We made use of antibiotic selection followed by cell sorting to select for Saos-2 cells stably transfected with GR★-GFP (see Supporting Information) and dubbed this new cell line Soas-2(GIGT).

To ensure that the GIGT assay could be performed in Saos-2(GIGT) cells, we treated cells for 30 min with or without 1 μM SDex and quantified translocation ratios (TR) using an Opera high-content imaging system and Acapella High Content Imaging and Analysis software (Perkin-Elmer). In the absence of SDex, GR★-GFP distributes nearly uniformly throughout the cytosol and nucleus (Figure 6a), resulting in an average TR

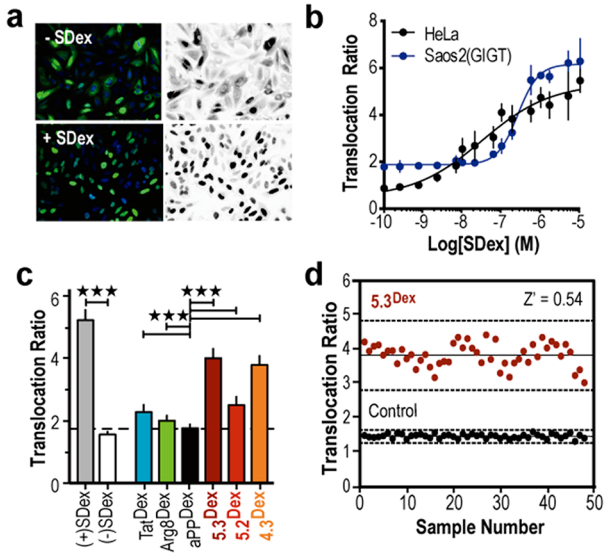

Figure 6. GIGT validation in stably transfected Saos-2(GIGT) cells. (a) Images of Saos-2(GIGT) cells stably transfected with GR★-GFP with or without treatment with 1 μM SDex for 30 min. Left images show an overlay of GFP signal (green) with Hoechst 33342 (blue) and right images display GFP signal in grayscale. (b) Effect of SDex on the calculated TR in HeLa cells transiently transfected with GR★-GFP and stable Saos-2(GIGT) cells. (c) Analysis of GR★-GFP nuclear translocation in Saos-2(GIGT) cells after a 30 min treatment with 1 μM SDex or Dex-labeled peptides. TRs, expressed ± standard deviation, were calculated using Acapella (see Supporting Information). *** $p \leq 0.001$; ANOVA. (d) Well-to-well variability of GIGT in Saos-2(GIGT) cells treated for 30 min with 1 μM 5.3^{Dex} or without (control). TR values calculated described were randomized and plotted as a function of sample number; $n = 50$. Solid lines represent mean TRs for treated or untreated cells. Dashed lines represent mean value ±3 times the standard deviation (Excel). The Z'-factor[38] was calculated using eq 3 (see Experimental Procedures).

of 1.48 ± 0.06. In the presence of 1 μM SDex, GR★-GFP translocates almost exclusively to the nucleus, with a resultant ratio of 5.11 ± 0.34. The TR calculated for Saos-2(GIGT) cells treated with 1 μM SDex (5.68 ± 0.13) are higher and less variable than those for equivalently treated, transiently transfected HeLa cells (4.74 ± 0.42) (Figure 6b). This improvement in signal and reduction in variability supports the use of Saos-2(GIGT) cells over transiently transfected HeLa cells for high-content GIGT analysis.

dx.doi.org/10.1021/bi401069g | Biochemistry XXXX, XXX, XXX−XXX

Next, we made use of Saos-2(GIGT) cells to compare the relative cytosolic delivery of Dex-tagged peptides such as Tat,[56] Arg_8,[59] and a panel of previously examined, minimally cationic polypeptides[34] (Figure 6c). We observed significant GR★-GFP nuclear translocation when Saos-2(GIGT) cells were treated with 1 μM 5.3^{Dex}, 4.3^{Dex}, and 5.2^{Dex}, with the highest TRs observed in the presence of 5.3^{Dex}. In contrast to GIGT performance in transiently transfected HeLa cells, where significant TRs were measured only for 5.3^{Dex} (Figure 5c), in Saos-2(GIGT) cells significant TRs were measured for both 5.3^{Dex} (4.01 ± 0.30) and 4.3^{Dex} (3.79 ± 0.29). Low TRs are observed for both Tat^{Dex} (2.28 ± 0.24) and Arg_8^{Dex} (2.00 ± 0.16). The discrepancies in miniature protein TR values may result from the differential modes of endocytic uptake between the two cell lines, as the endocytic regulatory network is cell-type dependent.[64,65]

Finally, to identify the applicability of Saos-2(GIGT) cells to high-throughput microscopy, we calculated the Z'-factor[38] (see Experimental Procedures, eq 3) across 50 experimental populations of over 200 cells. The Z'-factor between Saos-2(GIGT) cells treated in the presence and absence of 1 μM 5.3^{Dex} was 0.54 (Figure 6d), which indicates that GIGT is a robust platform for high-throughput screening of Dex-peptide conjugates.

Evaluating Cytosolic Delivery of Zinc-Finger Domains. Zinc-finger nucleases (ZFNs) are fusion proteins composed of restriction endonucleases and Cys_2-His_2 zinc-finger domains[66,67] that have displayed potential as agents for targeted gene therapy.[25,68,69] The modular zinc-finger components can be customized to target specific gene sequences, enabling ZFNs to induce site-specific double-strand DNA breaks that knock out gene function upon nonhomologous recombination.[21,22,25] There is little doubt that the utility of ZFNs would be enhanced if they could be delivered directly into the interior of living cells without the use of retroviral insertion. Although attempts to enhance ZFN uptake by appending highly cationic peptide sequences, such as Tat or Arg_8, have met with only modest success,[21] it was recently reported that certain ZFNs reach the cell interior without further modification,[21] perhaps because their DNA binding domains carry a net positive charge.[21,25] Notably, the assay used to detect the ZFN in this case is exceedingly sensitive, requiring in the limiting case only a single ZFN-catalyzed nonhomologous recombination event to generate a positive signal.

We used both GIGI and GIGT to compare the relative cytosolic localization of an unmodified zinc-finger domain (wtZF) to that of ZF5.3[34] and the four ZFNs reported recently to enter the interior of mammalian cells, ZFN1−4.[21] Variants of ZFN1−4 carrying a C-terminal Dex tag were prepared by solid phase synthesis[21] (Figure 7a and b; see Supporting Information). All zinc-finger domains showed evidence of α-helical structure at a concentration of 25 μM (10 mM, Tris at pH 7.4) in the presence of 50 μM $ZnCl_2$ when measured by circular dichroism spectroscopy; wtZF, ZF5.3, ZFN4, and ZFN2 showed the highest levels of helical structure (Figure S9, Supporting Information).

We then used GIGI (Figure 7c) and GIGT (Figure 7d) to compare the cytosolic localization of all six zinc finger domains in stably transfected U2OS(GIGI) and Saos2(GIGT) cells. $ZF5.3^{Dex}$ induced sigificantly higher levels of eGFP expression (GIGI) and GR★-GFP translocation (GIGT) than wtZF and all four ZFN domains tested. When analyzed after cell lysis, $ZF5.3^{Dex}$ induced eGFP expression in U2OS(GIGI) cells with

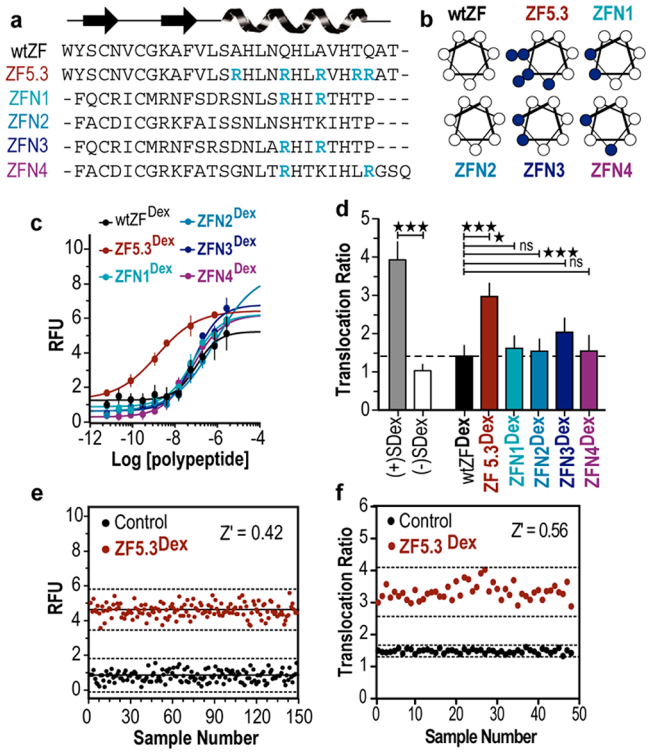

Figure 7. Analysis of natural and engineered ZF domains using GIGI and GIGT. (a) Primary sequences of zinc finger domains evaluated herein; α-helical arginine residues are colored blue. (b) Helical wheel diagrams of each ZF domain illustrating the relative location of each α-helical arginine residue, which is represented as a blue circle. (c) GIGI in cell lysates: concentration-dependent effect of each Dex-labeled ZF domain on eGFP expression in U2OS(GIGI) cells after 24 h of treatment. EC_{50} values are shown in Table S2, Supporting Information. RFUs, expressed ± standard deviation, were calculated and curve fits performed as described (see Experimental Procedures). (d) Analysis of GR★-GFP nuclear translocation in transiently transfected HeLa cells treated with or without 500 nM SDex or Dex-labeled ZF proteins for 30 min. TRs, expressed ± standard deviation, were calculated using CellProfiler as previously reported[34] (see Supporting Information). * $p \leq 0.05$; *** $p \leq 0.001$; ns, not significant, ANOVA. (e) GIGI in cell lysates. Well-to-well variability of GIGI in U2OS(GIGI) cells treated for 24 h with or without (control) 1 μM $ZF5.3^{Dex}$. RFU values were calculated as described above, randomized, and plotted as a function of sample number; n = 150. Solid lines represent mean RFUs for treated or untreated cells. Dashed lines represent the mean value ±3 times the standard deviation. (f) Well-to-well variability of GIGT in Saos-2(GIGT) cells treated for 30 min with or without (control) 1 μM $ZF5.3^{Dex}$. TR values were calculated using Acapella image analysis software as described and plotted as a function of sample number; n = 48. Solid lines represent mean TRs for treated or untreated cells. Dashed lines represent the mean value ±3 times the standard deviation (Excel). Z'-factors[38] were calculated using eq 3 (see Experimental Procedures).

an EC_{50} a full 100-fold lower than that of $wtZF^{Dex}$ (1.4 nM vs 102.7 nM) (Figure 7c and Table S3, Supporting Information) and 70−80-fold lower than that of ZF domains $ZFN1-4^{Dex}$. Similar trends are observed when cytosolic entry is evaluated using GIGT (Figure 7d). Significant differences are also observed when the ZF domains are compared across cell populations: the most active ZFN reported induced eGFP expression in only 12% of the cells treated,[21] whereas $ZF5.3^{Dex}$ led to significant translocation ratios in greater than 99% of cells expressing GR★-GFP. These results indicate that the

dx.doi.org/10.1021/bi401069g | Biochemistry XXXX, XXX, XXX−XXX

penta-Arg containing ZF5.3 trafficks to the cytosol more efficiently than ZF domains that lack a penta-Arg motif and that introduction of a penta-Arg motif significantly improves the cytosolic delivery of zinc finger nuclease domains.

To test the robustness of GIGI and GIGT assays for analyzing the relative trafficking of zinc-finger proteins, we measured the Z'-factor between U2OS(GIGI) and Saos-2(GIGT) cells treated in the presence and absence of 1 μM ZF5.3^{Dex} (Figure 7e and f). Notably, the Z'-factor[38] (see Experimental Procedures, eq 3) was determined to be 0.42 for the GIGI assay and 0.56 for the GIGT assay, which indicates that both GIGI and GIGT are robust enough to be used for high-throughput screening of cell populations treated with ZF5.3^{Dex}.

■ DISCUSSION

Proteins capable of crossing biological membranes show great promise as therapeutics as well as agents for delivery of macromolecules, such as siRNA, to the interior of mammalian cells.[70,71] In this work, we describe significant improvements to two assays that evaluate the intramembrane trafficking and cytosolic delivery of peptides and protein conjugates. The improvements we describe increase assay speed, sensitivity, and versatility, and decrease assay cost-per-well. One assay (GIGI) is based on an amplified read-out that informs on cytosolic delivery without the need for sophisticated imaging equipment or adherent cells. The second assay (GIGT) is based on a nonamplified read-out and informs on relative cytosolic delivery in a way that exploits the unique capabilities of sophisticated imaging equipment. With these assays, we showed definitively that both overall charge and charge distribution influence the efficiency of endosomal release into the cytosol and that inclusion of a helical, penta-Arg motif can dramatically increase the cytosolic delivery of small proteins and zinc finger domains.

How might these assays be used? One application combines the GIGT assay with an image-based, genome-wide interference screen to identify those gene products whose knockdown increases endosomal release and in this way identify those elements of the trafficking machinery that engage the penta-Arg motif. These studies could discover fundamentally new elements of cellular machinery and/or new molecular targets whose modulation by small molecules could further improve peptide/peptide mimetic function. A complementary application exploits the GIGI assay to sort large molecular libraries whose members contain variations on the penta-Arg motif to further improve cytosolic trafficking. In the fullness of time, these discoveries could help formulate a peptide/peptide mimetic variation on the rule-of-five to optimize the design of genuinely cell penetrating variants of molecules that are otherwise delivered genetically, such as zinc-finger nuclease and TALENs.

■ ASSOCIATED CONTENT

Supporting Information

Methods describing peptide synthesis and labeling, plasmid construction, cell culture, and transfections. This material is available free of charge via the Internet at http://pubs.acs.org.

■ AUTHOR INFORMATION

Corresponding Author

*Phone: 203-432-5094. E-mail: Alanna.schepartz@yale.edu.

Author Contributions

‖J.M.H. and J.R.L. contributed equally to this work.

Funding

This work was supported by US National Institutes of Health (NIH) grants R01 GM74756 and CA170741. J.R.L. gratefully acknowledges support from an NIH-funded Chemistry Biology Interface Training Program (T32GM067543); J.S.A. acknowledges support from NIH MSTP TG T32GM07205 and NIH F30 HL 09047803.

Notes

The authors declare no competing financial interest.

■ ACKNOWLEDGMENTS

We are grateful to Tom Kodadek for providing the pGal4DBD-GRLBD-VP16 plasmid.

■ REFERENCES

(1) Makley, L. N., and Gestwicki, J. E. (2013) Expanding the number of 'druggable' targets: non-enzymes and protein-protein interactions. *Chem. Biol. Drug Des. 81*, 22−32.

(2) Wells, J. A., and McClendon, C. L. (2007) Reaching for high-hanging fruit in drug discovery at protein-protein interfaces. *Nature 450*, 1001−1009.

(3) Garner, A. L., and Janda, K. D. (2011) Protein-protein interactions and cancer: targeting the central dogma. *Curr. Top. Med. Chem. 11*, 258−280.

(4) Fry, D. C. (2012) Small-molecule inhibitors of protein-protein interactions: how to mimic a protein partner. *Curr. Pharm. Des. 18*, 4679−4684.

(5) Filippakopoulos, P., Qi, J., Picaud, S., Shen, Y., Smith, W. B., Fedorov, O., Morse, E. M., Keates, T., Hickman, T. T., Felletar, I., Philpott, M., Munro, S., McKeown, M. R., Wang, Y., Christie, A. L., West, N., Cameron, M. J., Schwartz, B., Heightman, T. D., La Thangue, N., French, C. A., Wiest, O., Kung, A. L., Knapp, S., and Bradner, J. E. (2010) Selective inhibition of BET bromodomains. *Nature 468*, 1067−1073.

(6) Cai, Z., Greene, M. I., and Berezov, A. (2008) Modulation of biomolecular interactions with complex-binding small molecules. *Methods 46*, 39−46.

(7) Busschots, K., De Rijck, J., Christ, F., and Debyser, Z. (2009) In search of small molecules blocking interactions between HIV proteins and intracellular cofactors. *Mol. Biosyst. 5*, 21−31.

(8) Benyamini, H., and Friedler, A. (2010) Using peptides to study protein-protein interactions. *Future Med. Chem. 2*, 989−1003.

(9) Dewal, M. B., and Firestine, S. M. (2011) Non-peptidic alpha-helical mimetics as protein-protein interaction inhibitors. *Curr. Med. Chem. 18*, 2420−2428.

(10) Lipinski, C. A., Lombardo, F., Dominy, B. W., and Feeney, P. J. (2001) Experimental and computational approaches to estimate solubility and permeability in drug discovery and development settings. *Adv. Drug Delivery Rev. 46*, 3−26.

(11) Arkin, M. R., and Whitty, A. (2009) The road less traveled: modulating signal transduction enzymes by inhibiting their protein-protein interactions. *Curr. Opin. Chem. Biol. 13*, 284−290.

(12) Morelli, X., Bourgeas, R., and Roche, P. (2011) Chemical and structural lessons from recent successes in protein-protein interaction inhibition (2P2I). *Curr. Opin. Chem. Biol. 15*, 475−481.

(13) Ryser, H. J., and Hancock, R. (1965) Histones and basic polyamino acids stimulate the uptake of albumin by tumor cells in culture. *Science 150*, 501−503.

(14) Ryser, H. J. (1967) Studies on protein uptake by isolated tumor cells. 3. Apparent stimulations due to pH, hypertonicity, polycations, or dehydration and their relation to the enhanced penetration of infectious nucleic acids. *J. Cell Biol. 32*, 737−750.

(15) Verdine, G. L., and Hilinski, G. J. (2012) Stapled Peptides for Intracellular Drug Targets. *Methods Enzymol. 503*, 3−33.

(16) Bernal, F., Tyler, A. F., Korsmeyer, S. J., Walensky, L. D., and Verdine, G. L. (2007) Reactivation of the p53 tumor suppressor pathway by a stapled p53 peptide. *J. Am. Chem. Soc. 129*, 2456−2457.
(17) Walensky, L. D., Kung, A. L., Escher, I., Malia, T. J., Barbuto, S., Wright, R. D., Wagner, G., Verdine, G. L., and Korsmeyer, S. J. (2004) Activation of apoptosis in vivo by a hydrocarbon-stapled BH3 helix. *Science 305*, 1466−1470.
(18) McNaughton, B. R., Cronican, J. J., Thompson, D. B., and Liu, D. R. (2009) Mammalian cell penetration, siRNA transfection, and DNA transfection by supercharged proteins. *Proc. Natl. Acad. Sci. U.S.A. 106*, 6111−6116.
(19) Cronican, J. J., Thompson, D. B., Beier, K. T., McNaughton, B. R., Cepko, C. L., and Liu, D. R. (2010) Potent delivery of functional proteins into Mammalian cells in vitro and in vivo using a supercharged protein. *ACS Chem. Biol. 5*, 747−752.
(20) Thompson, D. B., Cronican, J. J., and Liu, D. R. (2012) Engineering and identifying supercharged proteins for macromolecule delivery into mammalian cells. *Methods Enzymol. 503*, 293−319.
(21) Gaj, T., Guo, J., Kato, Y., Sirk, S. J., and Barbas, C. F., III (2012) Targeted gene knockout by direct delivery of zinc-finger nuclease proteins. *Nat. Methods 9*, 805−807.
(22) Carroll, D. (2011) Genome engineering with zinc-finger nucleases. *Genetics 188*, 773−782.
(23) Handel, E. M., and Cathomen, T. (2011) Zinc-finger nuclease based genome surgery: it's all about specificity. *Curr. Gene Ther. 11*, 28−37.
(24) Hockemeyer, D., Soldner, F., Beard, C., Gao, Q., Mitalipova, M., DeKelver, R. C., Katibah, G. E., Amora, R., Boydston, E. A., Zeitler, B., Meng, X., Miller, J. C., Zhang, L., Rebar, E. J., Gregory, P. D., Urnov, F. D., and Jaenisch, R. (2009) Efficient targeting of expressed and silent genes in human ESCs and iPSCs using zinc-finger nucleases. *Nat. Biotechnol. 27*, 851−857.
(25) Young, J. J., and Harland, R. M. (2012) Targeted gene disruption with engineered zinc-finger nucleases (ZFNs). *Methods Mol. Biol. 917*, 129−141.
(26) Wender, P. A., and Miller, B. L. (2009) Synthesis at the molecular frontier. *Nature 460*, 197−201.
(27) Duchardt, F., Fotin-Mleczek, M., Schwarz, H., Fischer, R., and Brock, R. (2007) A comprehensive model for the cellular uptake of cationic cell-penetrating peptides. *Traffic 8*, 848−866.
(28) Varkouhi, A. K., Scholte, M., Storm, G., and Haisma, H. J. (2011) Endosomal escape pathways for delivery of biologicals. *J. Controlled Release 151*, 220−228.
(29) Johnson, J. R., Kocher, B., Barnett, E. M., Marasa, J., and Piwnica-Worms, D. (2012) Caspase-activated cell-penetrating peptides reveal temporal coupling between endosomal release and apoptosis in an RGC-5 cell model. *Bioconjugate Chem. 23*, 1783−1793.
(30) Salomone, F., Cardarelli, F., Di Luca, M., Boccardi, C., Nifosi, R., Bardi, G., Di Bari, L., Serresi, M., and Beltram, F. (2012) A novel chimeric cell-penetrating peptide with membrane-disruptive properties for efficient endosomal escape. *J. Controlled Release 163*, 293−303.
(31) Erazo-Oliveras, A., Muthukrishnan, N., Baker, R., Wang, T.-Y., and Pellois, J.-P. (2012) Improving the endosomal escape of cell-penetrating peptides and their cargos: strategies and challenges. *Pharmaceuticals 5*, 1177−1209.
(32) Daniels, D. S., and Schepartz, A. (2007) Intrinsically cell-permeable miniature proteins based on a minimal cationic PPII motif. *J. Am. Chem. Soc. 129*, 14578−14579.
(33) Smith, B. A., Daniels, D. S., Coplin, A. E., Jordan, G. E., McGregor, L. M., and Schepartz, A. (2008) Minimally cationic cell-permeable miniature proteins via alpha-helical arginine display. *J. Am. Chem. Soc. 130*, 2948−2949.
(34) Appelbaum, J. S., Larochelle, J. R., Smith, B. A., Balkin, D. M., Holub, J. M., and Schepartz, A. (2012) Arginine topology controls escape of minimally cationic proteins from early endosomes to the cytoplasm. *Chem. Biol. 19*, 819−830.
(35) Carpenter, A. E., Jones, T. R., Lamprecht, M. R., Clarke, C., Kang, I. H., Friman, O., Guertin, D. A., Chang, J. H., Lindquist, R. A., Moffat, J., Golland, P., and Sabatini, D. M. (2006) CellProfiler: image analysis software for identifying and quantifying cell phenotypes. *Genome Biol. 7*, R100.
(36) El Andaloussi, S., Guterstam, P., and Langel, U. (2007) Assessing the delivery efficacy and internalization route of cell-penetrating peptides. *Nat. Protoc. 2*, 2043−2047.
(37) Holm, T., Johansson, H., Lundberg, P., Pooga, M., Lindgren, M., and Langel, U. (2006) Studying the uptake of cell-penetrating peptides. *Nat. Protoc. 1*, 1001−1005.
(38) Zhang, J. H., Chung, T. D., and Oldenburg, K. R. (1999) A simple statistical parameter for use in evaluation and validation of high throughput screening assays. *J. Biomol. Screening 4*, 67−73.
(39) Schneider, C. A., Rasband, W. S., and Eliceiri, K. W. (2012) NIH Image to ImageJ: 25 years of image analysis. *Nat. Methods 9*, 671−675.
(40) Yu, P., Liu, B., and Kodadek, T. (2005) A high-throughput assay for assessing the cell permeability of combinatorial libraries. *Nat. Biotechnol. 23*, 746−751.
(41) Galigniana, M. D., Echeverria, P. C., Erlejman, A. G., and Piwien-Pilipuk, G. (2010) Role of molecular chaperones and TPR-domain proteins in the cytoplasmic transport of steroid receptors and their passage through the nuclear pore. *Nucleus 1*, 299−308.
(42) Grad, I., and Picard, D. (2007) The glucocorticoid responses are shaped by molecular chaperones. *Mol. Cell. Endocrinol. 275*, 2−12.
(43) Picard, D., and Yamamoto, K. R. (1987) Two signals mediate hormone-dependent nuclear localization of the glucocorticoid receptor. *EMBO J. 6*, 3333−3340.
(44) Beato, M. (1989) Gene regulation by steroid hormones. *Cell 56*, 335−344.
(45) Kwon, Y. U., and Kodadek, T. (2007) Quantitative evaluation of the relative cell permeability of peptoids and peptides. *J. Am. Chem. Soc. 129*, 1508−1509.
(46) Kwon, Y. U., and Kodadek, T. (2007) Quantitative comparison of the relative cell permeability of cyclic and linear peptides. *Chem. Biol. 14*, 671−677.
(47) Tan, N. C., Yu, P., Kwon, Y. U., and Kodadek, T. (2008) High-throughput evaluation of relative cell permeability between peptoids and peptides. *Bioorg. Med. Chem. 16*, 5853−5861.
(48) Auld, D. S., Thorne, N., Nguyen, D. T., and Inglese, J. (2008) A specific mechanism for nonspecific activation in reporter-gene assays. *ACS Chem. Biol. 3*, 463−470.
(49) Chakraborti, P. K., Garabedian, M. J., Yamamoto, K. R., and Simons, S. S., Jr. (1991) Creation of "super" glucocorticoid receptors by point mutations in the steroid binding domain. *J. Biol. Chem. 266*, 22075−22078.
(50) Chakraborti, P. K., Garabedian, M. J., Yamamoto, K. R., and Simons, S. S., Jr. (1992) Role of cysteines 640, 656, and 661 in steroid binding to rat glucocorticoid receptors. *J. Biol. Chem. 267*, 11366−11373.
(51) Kucera, T., Waltner-Law, M., Scott, D. K., Prasad, R., and Granner, D. K. (2002) A point mutation of the AF2 transactivation domain of the glucocorticoid receptor disrupts its interaction with steroid receptor coactivator 1. *J. Biol. Chem. 277*, 26098−26102.
(52) Sarlis, N. J., Bayly, S. F., Szapary, D., and Simons, S. S., Jr. (1999) Quantity of partial agonist activity for antiglucocorticoids complexed with mutant glucocorticoid receptors is constant in two different transactivation assays but not predictable from steroid structure. *J. Steroid Biochem. Mol. Biol. 68*, 89−102.
(53) DeFilippis, R. A., Goodwin, E. C., Wu, L., and DiMaio, D. (2003) Endogenous human papillomavirus E6 and E7 proteins differentially regulate proliferation, senescence, and apoptosis in HeLa cervical carcinoma cells. *J. Virol. 77*, 1551−1563.
(54) Fingar, D. C., Salama, S., Tsou, C., Harlow, E., and Blenis, J. (2002) Mammalian cell size is controlled by mTOR and its downstream targets S6K1 and 4EBP1/eIF4E. *Genes Dev. 16*, 1472−1487.
(55) McClure, L. V., Seo, G. J., and Sullivan, C. S. (2011) Reporter-based assays for analyzing RNA interference in mammalian cells. *Methods Mol. Biol. 725*, 173−189.

(56) Frankel, A. D., and Pabo, C. O. (1988) Cellular uptake of the tat protein from human immunodeficiency virus. *Cell 55*, 1189−1193.
(57) Koren, E., Apte, A., Sawant, R. R., Grunwald, J., and Torchilin, V. P. (2011) Cell-penetrating TAT peptide in drug delivery systems: proteolytic stability requirements. *Drug Delivery 18*, 377−384.
(58) Vives, E., Brodin, P., and Lebleu, B. (1997) A truncated HIV-1 Tat protein basic domain rapidly translocates through the plasma membrane and accumulates in the cell nucleus. *J. Biol. Chem. 272*, 16010−16017.
(59) Mitchell, D. J., Kim, D. T., Steinman, L., Fathman, C. G., and Rothbard, J. B. (2000) Polyarginine enters cells more efficiently than other polycationic homopolymers. *J. Peptide Res. 56*, 318−325.
(60) Jones, A. T., and Sayers, E. J. (2012) Cell entry of cell penetrating peptides: tales wagging dogs. *J. Controlled Release 161*, 582−591.
(61) Hitz, T., Iten, R., Gardiner, J., Namoto, K., Walde, P., and Seebach, D. (2006) Interaction of alpha-and beta-oligoarginine-acids and amides with anionic lipid vesicles: a mechanistic and thermodynamic study. *Biochemistry 45*, 5817−5829.
(62) Luedtke, N. W., Dexter, R. J., Fried, D. B., and Schepartz, A. (2007) Surveying polypeptide and protein domain conformation and association with FlAsH and ReAsH. *Nat. Chem. Biol. 3*, 779−784.
(63) Xu, G. W., Mawji, I. A., Macrae, C. J., Koch, C. A., Datti, A., Wrana, J. L., Dennis, J. W., and Schimmer, A. D. (2008) A high-content chemical screen identifies ellipticine as a modulator of p53 nuclear localization. *Apoptosis 13*, 413−422.
(64) Doherty, G. J., and McMahon, H. T. (2009) Mechanisms of endocytosis. *Annu. Rev. Biochem. 78*, 857−902.
(65) Mercer, J., and Helenius, A. (2009) Virus entry by macropinocytosis. *Nat. Cell Biol. 11*, 510−520.
(66) Kim, Y. G., Cha, J., and Chandrasegaran, S. (1996) Hybrid restriction enzymes: zinc finger fusions to Fok I cleavage domain. *Proc. Natl. Acad. Sci. U.S.A. 93*, 1156−1160.
(67) Kim, Y. G., and Chandrasegaran, S. (1994) Chimeric restriction endonuclease. *Proc. Natl. Acad. Sci. U.S.A. 91*, 883−887.
(68) Perez, E. E., Wang, J., Miller, J. C., Jouvenot, Y., Kim, K. A., Liu, O., Wang, N., Lee, G., Bartsevich, V. V., Lee, Y. L., Guschin, D. Y., Rupniewski, I., Waite, A. J., Carpenito, C., Carroll, R. G., Orange, J. S., Urnov, F. D., Rebar, E. J., Ando, D., Gregory, P. D., Riley, J. L., Holmes, M. C., and June, C. H. (2008) Establishment of HIV-1 resistance in CD4+ T cells by genome editing using zinc-finger nucleases. *Nat. Biotechnol. 26*, 808−816.
(69) Perez-Pinera, P., Ousterout, D. G., and Gersbach, C. A. (2012) Advances in targeted genome editing. *Curr. Opin. Chem. Biol. 16*, 268−277.
(70) Wender, P. A., Cooley, C. B., and Geihe, E. I. (2012) Beyond cell penetrating peptides: designed molecular transporters. *Drug Discovery Today Technol. 9*, e49−e55.
(71) Chugh, A., Eudes, F., and Shim, Y. S. (2010) Cell-penetrating peptides: Nanocarrier for macromolecule delivery in living cells. *IUBMB Life 62*, 183−193.

dx.doi.org/10.1021/bi401069g | *Biochemistry* XXXX, XXX, XXX−XXX